

# A NEW METHOD FOR TOPOLOGY DESIGN OF ELECTROMAGNETIC ANTENNAS IN HYPERTHERMIA THERAPY

A.A.S AMAD, A.F.D. LOULA AND A.A. NOVOTNY

ABSTRACT. The topological derivative concept has been proved to be useful in many relevant applications such as topology optimization, inverse problems, image processing, multi-scale constitutive modeling, fracture mechanics and damage evolution modeling. In this work, we develop a new optimization method based on the topological derivative concept applied to the cancer treatment by hyperthermia. Hyperthermia therapy is a non-invasive medical treatment in which body tissue is artificially heated through electromagnetic waves, focusing the heat in cancerous cells undergoing apoptosis. The basic idea, therefore, consists in finding a distribution of heat source generated by electromagnetic antenna aiming to increase the temperature in the region occupied by the tumor, while keeping the temperature in the remainder part of the body. Numerical results are presented illustrating possible application of the proposed methodology to treatment of cancer by hyperthermia.

## 1. INTRODUCTION

Hyperthermia is a non-invasive therapy, commonly used in treatment of cancer, consisting in artificially heating body tissue through electromagnetic waves by focusing the heat in cancerous cells. It is based on the observed fact that the vessels in the normal tissues dilate when heated, increasing the blood flow and consequently allowing the appropriated regulation of their temperature [1, 2, 3]. In contrast, cancerous tissues have a very disorganized and compact vascular structure, reducing the dissipation of the delivered heat by blood flow, so that the intra-tumoral temperature tends to increase. Thus, the applied heat may damage or even kill first the cancerous cells. Even if the cancerous cells do not die immediately, they may become more vulnerable to radiotherapy or chemotherapy, enabling such – in general aggressive – therapies to be given in smaller doses [3]. However, one of the challenges in the hyperthermia treatment is to selectively heat the cancerous tissue, elevating its temperature above  $42^{\circ}C$ , while keeping the temperatures of the healthy tissue close to the normal temperature of the human body [1, 3, 4, 5]. Several optimization methods have been proposed to maximize the heat in the diseased tissue and, at the same time, to minimize the hot spots concentrated in the healthy tissue that arise in the treatment [6, 7, 8, 9, 10, 11, 12, 13, 14, 15, 16, 17].

The regional electromagnetic hyperthermia problem is modeled by a semi-coupled system of partial differential equations. The heat equation in biologic tissues, or *bioheat equation* [5, 18, 13, 19], is coupled with the *Helmholtz equation* [13, 19]. Electromagnetic waves are generated by spatially distributed antenna. This antenna produces a source in the Helmholtz equation, whose solution appears as a heat source in the bioheat equation. Therefore, the basic idea consists in finding a distribution of heat source generated by electromagnetic antenna, which is able to focus the heat into the tumor and keep the temperature under control in the healthy tissue [9, 16]. In particular, we are interested in the design of the support of the antenna, which leads to a topology optimization problem. There are many methods that could deal with such a problem like SIMP [20] and

---

*Key words and phrases.* topology design of antenna, topological derivatives, optimization method, regional hyperthermia, electromagnetic waves, treatment of cancer.

level-set [21], for instance. In this work we propose a new optimization method based on the topological derivative concept [22] to find the optimum configuration for the antenna.

The paper is organized as follows. The topology optimization problem is presented in Section 2. In Section 3 the topological derivative concept is introduced. In particular, arguments on the existence of the associated topological derivative together with its derivation in an explicit form are provided. Finally in Section 5 a fixed-point algorithm based on the resulting topological derivative is devised and some numerical experiments are presented, showing that the obtained antennas are able to selectively heat the target. The paper ends with some concluding remarks in Section 6.

## 2. TOPOLOGY OPTIMIZATION PROBLEM

Let us consider an open and bounded domain  $\Omega \subset \mathbb{R}^2$  with a Lipschitz continuous boundary  $\partial\Omega$ . We introduce a subset  $\mathcal{B}$  of  $\Omega$  representing the body tissue. Let us also consider a subset  $\omega$  of  $\mathcal{W} = \Omega \setminus \overline{\mathcal{B}}$  representing the antenna that emit electromagnetic waves, where the region  $\mathcal{W} \setminus \overline{\omega}$  in general is filled with deionized water. Our goal is to maximize the temperature in the diseased tissue  $\mathcal{D} \subset \mathcal{B}$  with respect to the support of the antenna  $\omega$ , while keeping the temperature in the healthy tissue  $\mathcal{B} \setminus \overline{\mathcal{D}}$  close to normal. See sketch in Fig. 1.

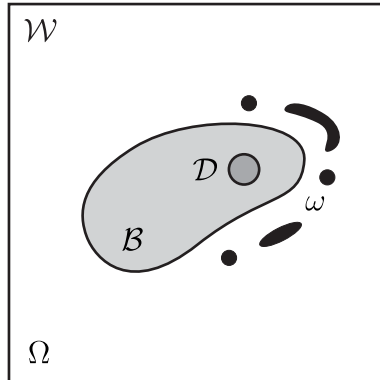


FIGURE 1. Original problem setting: domain  $\Omega$  and the original antenna  $\omega \subset \mathcal{W}$ , where  $\mathcal{D} \subset \mathcal{B}$  and  $\mathcal{B} \setminus \overline{\mathcal{D}}$  are the diseased and healthy tissues, respectively.

Let us introduce the model problem we are dealing with, which is given by a semi-coupled system of variational problems [13, 5]. In particular, the temperature  $\theta$  is solution to the following steady-state heat transfer problem:

Find  $\theta \in \Theta(\Omega)$ , such that

$$\int_{\Omega} (\kappa \nabla \theta \cdot \nabla \eta + cw(\theta - \theta_b)\eta) dx = \frac{1}{2} \int_{\Omega} \sigma |u|^2 \eta dx, \quad \forall \eta \in \Theta_0(\Omega), \quad (2.1)$$

with the set  $\Theta(\Omega) = \{\phi \in H^1(\Omega) : \phi|_{\partial\Omega} = \theta_{\Gamma}\}$  and  $\Theta_0(\Omega) = H_0^1(\Omega)$ , where  $H^1(\Omega) = \{\phi \in L^2(\Omega) : \nabla \phi \in L^2(\Omega)^2\}$  and  $H_0^1(\Omega) = \{\phi \in H^1(\Omega) : \phi|_{\partial\Omega} = 0\}$  are real Hilbert spaces. The function  $u$  is solution to the following time-harmonic wave problem:

Find  $u \in \mathbf{H}^1(\Omega)$ , such that

$$\int_{\Omega} (\nabla u \cdot \nabla \bar{\eta} - k^2 u \bar{\eta}) dx + \mathbf{i} \int_{\partial\Omega} ku \bar{\eta} ds = \int_{\Omega} f \bar{\eta} dx + \int_{\partial\Omega} r \bar{\eta} ds, \quad \forall \eta \in \mathbf{H}^1(\Omega), \quad (2.2)$$

with  $\bar{\eta}$  used to denote the complex conjugate of  $\eta$  and  $\mathbf{H}^1(\Omega) = \{\phi \in \mathbf{L}^2(\Omega) : \nabla\phi \in \mathbf{L}^2(\Omega)^2\}$  a complex Hilbert space, where  $\mathbf{L}^2(\Omega)$  is the space of square-integrable complex functions.

Some terms in the above equations require explanations. The thermal conductivity is denoted by  $\kappa = \kappa(x)$  [ $\text{Wm}^{-1} \text{ }^\circ\text{C}^{-1}$ ],  $c = c(x)$  [ $\text{J kg}^{-1} \text{ }^\circ\text{C}^{-1}$ ] is the specific heat,  $w = w(x)$  [ $\text{kg m}^{-3} \text{ s}^{-1}$ ] is the perfusion rate,  $\theta_b = \theta_b(x)$  is the temperature of the background,  $\theta_\Gamma = \theta_\Gamma(x)$  is the temperature on  $\partial\Omega$  and  $\sigma = \sigma(x)$  [ $\text{Sm}^{-1}$ ] is the electrical conductivity. The wavenumber is denoted by  $k = k(x) = k_0\sqrt{\varepsilon_r(x)\mu_r(x)}$ , where  $k_0$  is the wavenumber in free space,  $\varepsilon_r(x)$  is the relative permittivity and  $\mu_r(x)$  is the relative permeability. In addition,  $\mathbf{i}$  is the imaginary unit, namely  $\mathbf{i} = \sqrt{-1}$ , and  $r = r(x)$  is a Robin boundary data on  $\partial\Omega$ , which degenerates to an ideal absorbing condition by setting  $r = 0$ . In particular, all distributed parameters in  $\Omega$  depending on  $x$  are considered piecewise constant functions assuming different values in each region described in Fig. 1. Finally, the function  $f = f(x)$  is a distributed source term in  $\Omega$  defined as:

$$f(x) = \begin{cases} f_0, & \text{if } x \in \omega, \\ 0, & \text{if } x \in \Omega \setminus \bar{\omega}, \end{cases} \quad (2.3)$$

where  $f_0$  is the electromagnetic intensity. Therefore, problem (2.2) is the weak form of the *Helmholtz equation* with Robin boundary condition, while problem (2.1) is the weak form of the *diffusive-reactive equation* with Dirichlet boundary condition. Equations (2.1) and (2.2) lead to a one way coupled system. Given the source term  $f$  and the Robin boundary data  $r$ , equation (2.2) can be solved for  $u$  independently of the temperature  $\theta$  solution of (2.1). Given the background temperature  $\theta_b$  and the Dirichlet boundary data  $\theta_\Gamma$ , then from  $u$  solution of (2.2), the temperature equation (2.1) can be solved for  $\theta$ .

Since the goal is to maximize the temperature in  $\mathcal{D} \subset \mathcal{B}$  and keep the temperature in  $\mathcal{B} \setminus \bar{\mathcal{D}}$  under control, the following shape functional is introduced

$$\mathcal{J}(\theta) = -\frac{\alpha}{|\mathcal{D}|} \int_{\mathcal{D}} \theta \, dx + \frac{1-\alpha}{|\mathcal{B}|} \int_{\mathcal{B} \setminus \bar{\mathcal{D}}} \theta \, dx, \quad (2.4)$$

where the weight  $0 < \alpha < 1$ . In particular, we set  $\alpha = 0.5$ , which represents a balance between each term of the shape functional (2.4). Thus, our minimization problem can be stated as

$$\text{Minimize}_{\omega \subset \mathcal{W}} \mathcal{J}(\theta), \quad (2.5)$$

where  $\theta$  is the solution of the semi-coupled system of variational equations (2.1)-(2.2). Therefore,  $\theta$  depends implicitly on  $\omega$ , namely  $\theta = \theta(\omega)$ . Let us explain better the shape functional (2.4). Note that there is no target temperature in our formulation. Therefore we can not control the temperature level during the optimization process. On the other hand, we have observed that the resulting topology optimization algorithm based on (2.5) becomes very well-conditioned, leading to a feasible solution in just a few iterations. In fact, after obtaining the optimal support for the antenna, the temperature level can be adjusted *a posteriori* by changing the intensity  $f_0$  of the source.

Our main challenge here is to find the source term  $f$  of the time harmonic wave equation which leads to the minimum of the shape functional (2.4). In the next section we present a methodology based on a topological sensitivity analysis to solve the optimization problem (2.5). To this end we need to introduce two nested adjoint problems. The first one is associated with the semi-coupled heat problem (2.1), that is:

Find  $\varphi \in H_0^1(\Omega)$ , such that,

$$\int_{\Omega} (\kappa \nabla \varphi \cdot \nabla \eta + cw \varphi \eta) \, dx = -\frac{\alpha}{|\mathcal{D}|} \int_{\mathcal{D}} \eta \, dx + \frac{1-\alpha}{|\mathcal{B}|} \int_{\mathcal{B} \setminus \bar{\mathcal{D}}} \eta \, dx, \quad \forall \eta \in H_0^1(\Omega). \quad (2.6)$$

While the other one is associated with the Helmholtz problem (2.2), namely:

Find  $v \in \mathbf{H}^1(\Omega)$ , such that

$$\int_{\Omega} (\nabla v \cdot \nabla \bar{\eta} - k^2 v \bar{\eta}) dx - i \int_{\partial\Omega} k v \bar{\eta} ds = \int_{\Omega} \sigma \varphi u \bar{\eta} dx, \quad \forall \eta \in \mathbf{H}^1(\Omega), \quad (2.7)$$

Note that now the adjoint Helmholtz problem (2.7) depends on the solution to the adjoint thermal problem (2.6). Of course, problem (2.7) also depends on the solution to (2.2), while problem (2.6) is independent of (2.1) due to the choice of the shape function (2.4).

**Remark 1.** *A realistic simulation of the cancer treatment by hyperthermia should consider a three dimensional phenomenon of very complex nature whose mathematical model is still an open question and deserves further investigations. How to measure material properties of in-vivo tissues is a challenging issue. These properties in general present a non-linear behavior with respect to the temperature, for instance. Our simplified setting is a two dimensional, linear and steady-state **model problem**, which is adopted here as a starting point to introduce a new optimization methodology with potential applications to more realistic models of cancer treatment by hyperthermia.*

### 3. TOPOLOGICAL SENSITIVITY ANALYSIS

The topological derivative measures the sensitivity of a given shape functional with respect to an infinitesimal singular domain perturbation, such as the insertion of holes, inclusions, source-terms or even cracks. The topological derivative was rigorously introduced in [23]. Since then, this concept has become a subject of intensive research. In fact, the topological derivative has proved to be extremely useful in the solution of a wide range of problems, such as topology optimization [24], inverse problems [25], image processing [26], multi-scale constitutive modeling [27] and fracture [28] and damage [29] mechanics. See, for example, the book by Novotny & Sokołowski 2013 [22].

To introduce these ideas, let us consider a characteristic function  $\chi = \mathbf{1}_{\Omega}$  associated to the domain  $\Omega$ . Suppose that  $\Omega$  is subject to a singular perturbation confined in a small ball  $B_{\varepsilon}(\hat{x})$  of size  $\varepsilon$  and center at  $\hat{x} \in \Omega$ , as shown in Fig. 2. We denote by  $\chi_{\varepsilon}(\hat{x})$  the characteristic function associated to the topologically perturbed domain. In the case of a perforation, for instance,  $\chi_{\varepsilon}(\hat{x}) = \mathbf{1}_{\Omega} - \mathbf{1}_{\overline{B_{\varepsilon}(\hat{x})}}$ , and the perforated domain is obtained as  $\Omega_{\varepsilon}(\hat{x}) = \Omega \setminus \overline{B_{\varepsilon}(\hat{x})}$ . Then, we assume that a given shape functional  $\psi(\chi_{\varepsilon}(\hat{x}))$ , associated to the topologically perturbed domain, admits the following topological asymptotic expansion

$$\psi(\chi_{\varepsilon}(\hat{x})) = \psi(\chi) + \rho(\varepsilon) D_T \psi(\hat{x}) + \mathcal{R}(\rho(\varepsilon)), \quad (3.1)$$

where  $\psi(\chi)$  is the shape functional associated to the original (unperturbed) domain,  $\rho(\varepsilon)$  is a positive function such that  $\rho(\varepsilon) \rightarrow 0$ , when  $\varepsilon \rightarrow 0$ , and  $\mathcal{R}(\rho(\varepsilon)) = o(\rho(\varepsilon))$  is the remainder. The function  $\hat{x} \mapsto D_T \psi(\hat{x})$  is called the topological derivative of  $\psi$  at  $\hat{x}$ . Therefore, this derivative can be seen as a first order correction of  $\psi(\chi)$  to approximate  $\psi(\chi_{\varepsilon}(\hat{x}))$ .

**3.1. Perturbed Problems.** Let us introduce the perturbed counterpart of the shape functional, which is given by

$$\psi(\chi_{\varepsilon}) := \mathcal{J}(\theta_{\varepsilon}) = -\frac{\alpha}{|\mathcal{D}|} \int_{\mathcal{D}} \theta_{\varepsilon} dx + \frac{1-\alpha}{|\mathcal{B}|} \int_{\mathcal{B} \setminus \overline{\mathcal{D}}} \theta_{\varepsilon} dx, \quad (3.2)$$

where the weight  $\alpha$  is the same as in (2.4) and  $\theta_{\varepsilon}$  is the temperature distribution solution of the perturbed hyperthermia problem:

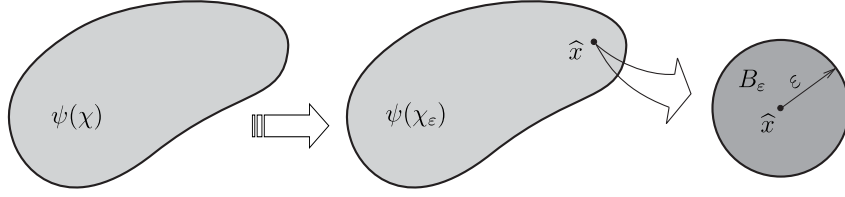


FIGURE 2. The topological derivative concept.

Find  $\theta_\varepsilon \in \Theta(\Omega)$ , such that

$$\int_{\Omega} (\kappa \nabla \theta_\varepsilon \cdot \nabla \eta + c w(\theta_\varepsilon - \theta_b) \eta) dx = \frac{1}{2} \int_{\Omega} \sigma |u_\varepsilon|^2 \eta dx, \quad \forall \eta \in \Theta_0(\Omega) \quad (3.3)$$

with  $u_\varepsilon$  solution to:

Find  $u_\varepsilon \in \mathbf{H}^1(\Omega)$ , such that

$$\int_{\Omega} (\nabla u_\varepsilon \cdot \nabla \bar{\eta} - k^2 u_\varepsilon \bar{\eta}) dx + i \int_{\partial \Omega} k u_\varepsilon \bar{\eta} ds = \int_{\Omega} f_\varepsilon \bar{\eta} dx + \int_{\partial \Omega} r \bar{\eta} ds, \quad \forall \eta \in \mathbf{H}^1(\Omega). \quad (3.4)$$

Here,  $f_\varepsilon$  is the perturbed source term which plays a fundamental role in our minimization problem. As we consider the source term as a piecewise constant function, the support of  $f$  becomes our key control variable. The topological sensitive analysis is used to find the optimal distribution of the antennas, or the support of the source function  $f$ . A perturbation in the source term is introduced by adding a piece of antenna outside  $\omega$  (where there is no antenna) or by removing a piece of antenna inside  $\omega$  (where there already exists an antenna) as illustrated in Fig. 3. Let us consider  $\hat{x} = (x^+, x^-)$ , with  $x^+ \in \mathcal{W} \setminus \bar{\omega}$  and  $x^- \in \omega$ . Then we introduce the perturbations  $B_\varepsilon(x^+) \subset \mathcal{W} \setminus \bar{\omega}$  and  $B_\varepsilon(x^-) \subset \omega$ , such that  $B_\varepsilon(x^+) \cap B_\varepsilon(x^-) = \emptyset$ . From these elements the perturbed source term  $f_\varepsilon$  is introduced as:

$$f_\varepsilon(x) = \begin{cases} f_0, & \text{if } x \in \omega_\varepsilon \\ 0, & \text{if } x \in \Omega \setminus \bar{\omega}_\varepsilon, \end{cases} \quad (3.5)$$

with  $\omega_\varepsilon = (\omega \setminus \overline{B_\varepsilon(x^-)}) \cup B_\varepsilon(x^+)$ . Note that for  $\varepsilon = 0$ ,  $\psi(\chi) := \mathcal{J}(\theta)$  in equation (2.4).

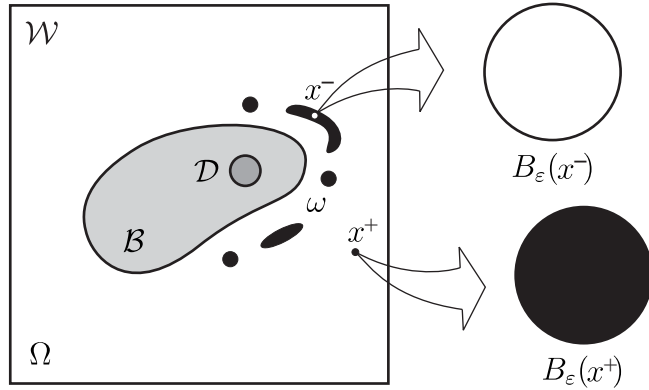


FIGURE 3. Perturbed problem setting: domain  $\Omega$  and the topologically perturbed antenna  $\omega_\varepsilon \subset \mathcal{W}$ , where  $\mathcal{D} \subset \mathcal{B}$  and  $\mathcal{B} \setminus \mathcal{D}$  are the diseased and healthy tissues, respectively.

**3.2. Stability with Respect to Topological Perturbations .** In this section we show that the solution of problem (3.4) is stable with respect to the size  $\varepsilon$  of the topological perturbation. Our stability analysis of the time harmonic wave equation is based on the following result from Melenk and Sauter [30, 31, 32].

**Proposition 2.** *Let  $\Omega$  be a bounded star-shaped domain with smooth boundary or a bounded convex domain. Then, there is  $C(\Omega) > 0$  such that for any  $f \in \mathbf{L}^2(\Omega)$ ,  $r \in \mathbf{H}^{1/2}(\partial\Omega)$ , the solution  $u$  of problem (2.2) satisfies*

$$\|u\|_{\mathcal{H}(\Omega)} \leq C(\Omega)(\|f\|_{\mathbf{L}^2(\Omega)} + \|r\|_{\mathbf{L}^2(\partial\Omega)}), \quad (3.6)$$

where the constant  $C(\Omega)$  is proportional to the diameter of  $\Omega$  and the norm  $\|p\|_{\mathcal{H}(\Omega)} := (p, p)_{\mathcal{H}}^{1/2}$ , which is equivalent to the usual  $\mathbf{H}^1(\Omega)$ -norm, is induced by the inner product

$$(p, q)_{\mathcal{H}} := \int_{\Omega} \nabla p \cdot \nabla \bar{q} \, dx + \int_{\Omega} k^2 p \bar{q} \, dx, \quad \forall p, q \in \mathbf{H}^1(\Omega).$$

**Lemma 3.** *Let  $\tilde{u}_{\varepsilon} = u_{\varepsilon} - u$ , where  $u$  and  $u_{\varepsilon}$  are solutions of (2.2) and (3.4), respectively. Then, we have the following estimate for  $\tilde{u}_{\varepsilon}$*

$$\|\tilde{u}_{\varepsilon}\|_{\mathcal{H}(\Omega)} \leq C\varepsilon^2, \quad (3.7)$$

where  $C$  is a constant independent of the small parameter  $\varepsilon$ .

*Proof.* Subtracting (2.2) from (3.4) we obtain

$$\begin{aligned} \tilde{u}_{\varepsilon} \in \mathbf{H}^1(\Omega) : \int_{\Omega} (\nabla \tilde{u}_{\varepsilon} \cdot \nabla \bar{\eta} - k^2 \tilde{u}_{\varepsilon} \bar{\eta}) \, dx + \mathbf{i} \int_{\partial\Omega} k \tilde{u}_{\varepsilon} \bar{\eta} \, ds = \\ \int_{B_{\varepsilon}(x^+)} f_0 \bar{\eta} \, dx - \int_{B_{\varepsilon}(x^-)} f_0 \bar{\eta} \, dx, \quad \forall \eta \in \mathbf{H}^1(\Omega), \end{aligned} \quad (3.8)$$

where we have used the definition of the perturbed source-term given by (3.5). In fact,

$$\begin{aligned} \int_{\omega_{\varepsilon}} f_0 \bar{\eta} \, dx &= \int_{\omega \setminus \overline{B_{\varepsilon}(x^-)}} f_0 \bar{\eta} \, dx + \int_{B_{\varepsilon}(x^+)} f_0 \bar{\eta} \, dx \\ &= \int_{\omega} f_0 \bar{\eta} \, dx - \int_{B_{\varepsilon}(x^-)} f_0 \bar{\eta} \, dx + \int_{B_{\varepsilon}(x^+)} f_0 \bar{\eta} \, dx, \end{aligned} \quad (3.9)$$

Let us introduce the following decomposition for  $\tilde{u}_{\varepsilon}$ , solution of (3.8),

$$\tilde{u}_{\varepsilon} = p_{\varepsilon} + q_{\varepsilon}. \quad (3.10)$$

Function  $p_{\varepsilon}$  is solution to

$$\begin{aligned} p_{\varepsilon} \in \mathbf{H}^1(\Omega) : \int_{\Omega} \nabla p_{\varepsilon} \cdot \nabla \bar{\eta} \, dx + \mathbf{i} \int_{\partial\Omega} k p_{\varepsilon} \bar{\eta} \, ds = \\ \int_{B_{\varepsilon}(x^+)} f_0 \bar{\eta} \, dx - \int_{B_{\varepsilon}(x^-)} f_0 \bar{\eta} \, dx, \quad \forall \eta \in \mathbf{H}^1(\Omega), \end{aligned} \quad (3.11)$$

while  $q_{\varepsilon}$  has to compensate for the discrepancy left by  $p_{\varepsilon}$ . Therefore, it is solution to the following problem

$$\begin{aligned} q_{\varepsilon} \in \mathbf{H}^1(\Omega) : \int_{\Omega} (\nabla q_{\varepsilon} \cdot \nabla \bar{\eta} - k^2 q_{\varepsilon} \bar{\eta}) \, dx + \\ \mathbf{i} \int_{\partial\Omega} k q_{\varepsilon} \bar{\eta} \, ds = \int_{\Omega} k^2 p_{\varepsilon} \bar{\eta} \, dx, \quad \forall \eta \in \mathbf{H}^1(\Omega). \end{aligned} \quad (3.12)$$

By setting  $\eta = p_\varepsilon$  as test function in (3.11) we obtain the following equality

$$\int_{\Omega} \nabla p_\varepsilon \cdot \nabla \bar{p}_\varepsilon \, dx + \mathbf{i} \int_{\partial\Omega} k p_\varepsilon \bar{p}_\varepsilon \, ds = \int_{B_\varepsilon(x^+)} f_0 \bar{p}_\varepsilon \, dx - \int_{B_\varepsilon(x^-)} f_0 \bar{p}_\varepsilon \, dx. \quad (3.13)$$

The Cauchy-Schwarz inequality yields

$$\int_{\Omega} \nabla p_\varepsilon \cdot \nabla \bar{p}_\varepsilon \, dx + \mathbf{i} \int_{\partial\Omega} k p_\varepsilon \bar{p}_\varepsilon \, ds \leq C_1 \varepsilon \left( \|p_\varepsilon\|_{\mathbf{L}^2(B_\varepsilon(x^+))} + \|p_\varepsilon\|_{\mathbf{L}^2(B_\varepsilon(x^-))} \right). \quad (3.14)$$

In addition, by making use of the Hölder inequality together with the Sobolev embedding theorem for  $1/p + 1/q = 1$  and  $q \geq 1$  [33, Ch. IV, §8, Sec. 1.2, pp 140], we have

$$\|p_\varepsilon\|_{\mathbf{L}^2(B_\varepsilon(x^+))} \leq A_1 \varepsilon^{1/q} \|p_\varepsilon\|_{\mathbf{L}^{2p}(B_\varepsilon(x^+))} \leq \varepsilon A_2 \|p_\varepsilon\|_{\mathbf{H}^1(\Omega)}, \quad (3.15)$$

$$\|p_\varepsilon\|_{\mathbf{L}^2(B_\varepsilon(x^-))} \leq B_1 \varepsilon^{1/q} \|p_\varepsilon\|_{\mathbf{L}^{2p}(B_\varepsilon(x^-))} \leq \varepsilon B_2 \|p_\varepsilon\|_{\mathbf{H}^1(\Omega)}, \quad (3.16)$$

where we have used the interior elliptic regularity of function  $p_\varepsilon$ . Therefore,

$$\int_{\Omega} \nabla p_\varepsilon \cdot \nabla \bar{p}_\varepsilon \, dx + \mathbf{i} \int_{\partial\Omega} k p_\varepsilon \bar{p}_\varepsilon \, ds \leq C_2 \varepsilon^2 \|p_\varepsilon\|_{\mathbf{H}^1(\Omega)}. \quad (3.17)$$

From the coercivity of the bilinear form on the left hand side of the above inequality and by the equivalence between the norms, we obtain

$$c \|p_\varepsilon\|_{\mathbf{H}^1(\Omega)}^2 \leq C_2 \varepsilon^2 \|p_\varepsilon\|_{\mathbf{H}^1(\Omega)} \quad \Rightarrow \quad \|p_\varepsilon\|_{\mathcal{H}(\Omega)} \leq C_3 \varepsilon^2, \quad (3.18)$$

with constant  $C_3$  independent of  $\varepsilon$ . Now, by setting  $f = k^2 p_\varepsilon$  and  $r = 0$  in Proposition 2, the following estimate for  $q_\varepsilon$ , solution to (3.12), holds true

$$\|q_\varepsilon\|_{\mathcal{H}(\Omega)} \leq C_4 \|k^2 p_\varepsilon\|_{\mathbf{L}^2(\Omega)} \leq C_5 \|p_\varepsilon\|_{\mathcal{H}(\Omega)} \leq C_6 \varepsilon^2, \quad (3.19)$$

where we have used (3.18). Finally, from the above estimates, the triangular inequality in (3.10) yields

$$\|\tilde{u}_\varepsilon\|_{\mathcal{H}(\Omega)} \leq C_7 (\|p_\varepsilon\|_{\mathcal{H}(\Omega)} + \|q_\varepsilon\|_{\mathcal{H}(\Omega)}) \leq C \varepsilon^2, \quad (3.20)$$

which leads to the result, with the constant  $C$  independent of the small parameter  $\varepsilon$ .  $\square$

**3.3. The Topological Derivative .** As observed in Section 3, the topological sensitivity analysis provides an asymptotic expansion in the form of (3.1) for a given shape functional, whose main term, called topological derivative, measures the sensitivity of this functional when an infinitesimal singular perturbation is introduced at an arbitrary point of the domain [22]. To derive an explicit form for the topological derivative, we subtract (2.4) from (3.2), yielding

$$\mathcal{J}(\theta_\varepsilon) - \mathcal{J}(\theta) = -\frac{\alpha}{|\mathcal{D}|} \int_{\mathcal{D}} (\theta_\varepsilon - \theta) \, dx + \frac{1-\alpha}{|\mathcal{B}|} \int_{\mathcal{B} \setminus \bar{\mathcal{D}}} (\theta_\varepsilon - \theta) \, dx. \quad (3.21)$$

Now, we subtract (2.1) from (3.3), to obtain

$$\int_{\Omega} (\kappa \nabla(\theta_\varepsilon - \theta) \cdot \nabla \eta + cw(\theta_\varepsilon - \theta)\eta) \, dx = \frac{1}{2} \int_{\Omega} \sigma(|u_\varepsilon|^2 - |u|^2) \eta \, dx \quad \forall \eta \in H_0^1(\Omega), \quad (3.22)$$

Setting  $\eta = \varphi$  in the above equation we get

$$\int_{\Omega} (\kappa \nabla(\theta_\varepsilon - \theta) \cdot \nabla \varphi + cw(\theta_\varepsilon - \theta)\varphi) \, dx = \frac{1}{2} \int_{\Omega} \sigma(|u_\varepsilon|^2 - |u|^2) \varphi \, dx. \quad (3.23)$$

On the other hand, by setting  $\eta = \theta_\varepsilon - \theta$  in the adjoint heat problem (2.6), we obtain

$$\int_{\Omega} (\kappa \nabla \varphi \cdot \nabla(\theta_\varepsilon - \theta) + cw\varphi(\theta_\varepsilon - \theta)) \, dx = -\frac{\alpha}{|\mathcal{D}|} \int_{\mathcal{D}} (\theta_\varepsilon - \theta) \, dx + \frac{1-\alpha}{|\mathcal{B}|} \int_{\mathcal{B} \setminus \bar{\mathcal{D}}} (\theta_\varepsilon - \theta) \, dx. \quad (3.24)$$

Comparing the obtained results with (3.21) yields

$$\begin{aligned}\mathcal{J}(\theta_\varepsilon) - \mathcal{J}(\theta) &= \frac{1}{2} \int_{\Omega} \sigma(|u_\varepsilon|^2 - |u|^2) \varphi \, dx \\ &= \int_{\Omega} \sigma \varphi \Re\{u(\overline{u_\varepsilon - u})\} \, dx + \mathcal{E}_1(\varepsilon),\end{aligned}\quad (3.25)$$

where  $\Re\{\cdot\}$  denotes the real part of  $\{\cdot\}$  and the remainder  $\mathcal{E}_1(\varepsilon)$  is given by

$$\begin{aligned}\mathcal{E}_1(\varepsilon) &= \frac{1}{2} \int_{\Omega} \sigma |u_\varepsilon - u|^2 \varphi \, dx \\ &\leq C_1 \|u_\varepsilon - u\|_{\mathcal{H}(\Omega)}^2 = o(\varepsilon^2),\end{aligned}\quad (3.26)$$

where we have used the result from Lemma 3 together with the elliptic regularity of function  $\varphi$ . Now, we subtract (2.2) from (3.4), to obtain

$$\begin{aligned}\int_{\Omega} (\nabla(u_\varepsilon - u) \cdot \nabla \bar{\eta} - k^2(u_\varepsilon - u) \bar{\eta}) \, dx + \mathbf{i} \int_{\partial\Omega} k(u_\varepsilon - u) \bar{\eta} \, ds = \\ \int_{B_\varepsilon(x^+)} f_0 \bar{\eta} \, dx - \int_{B_\varepsilon(x^-)} f_0 \bar{\eta} \, dx, \quad \forall \eta \in \mathbf{H}^1(\Omega).\end{aligned}\quad (3.27)$$

By choosing  $\eta = v$  in the above equation, we have

$$\begin{aligned}\int_{\Omega} (\nabla(u_\varepsilon - u) \cdot \nabla \bar{v} - k^2(u_\varepsilon - u) \bar{v}) \, dx + \mathbf{i} \int_{\partial\Omega} k(u_\varepsilon - u) \bar{v} \, ds = \\ \int_{B_\varepsilon(x^+)} f_0 \bar{v} \, dx - \int_{B_\varepsilon(x^-)} f_0 \bar{v} \, dx.\end{aligned}\quad (3.28)$$

Let us now set  $\eta = u_\varepsilon - u$  in the adjoint Helmholtz problem (2.7), to get

$$\begin{aligned}\int_{\Omega} (\nabla v \cdot \nabla \overline{(u_\varepsilon - u)} - k^2 v \overline{(u_\varepsilon - u)}) \, dx - \mathbf{i} \int_{\partial\Omega} k v \overline{(u_\varepsilon - u)} \, ds = \\ \int_{\Omega} \sigma \varphi u \overline{(u_\varepsilon - u)} \, dx.\end{aligned}\quad (3.29)$$

By taking the real part of the last two equalities, we can compare the obtained result with (3.25), to obtain

$$\begin{aligned}\mathcal{J}(\theta_\varepsilon) - \mathcal{J}(\theta) &= \int_{B_\varepsilon(x^+)} f_0 \Re\{\bar{v}\} \, dx - \int_{B_\varepsilon(x^-)} f_0 \Re\{\bar{v}\} \, dx + \mathcal{E}_1(\varepsilon) \\ &= |B_\varepsilon(x^+)| f_0 \Re\{v(x^+)\} - |B_\varepsilon(x^-)| f_0 \Re\{v(x^-)\} + \mathcal{E}(\varepsilon),\end{aligned}\quad (3.30)$$

since  $\Re\{\bar{v}\} = \Re\{v\}$ . The remainder  $\mathcal{E}(\varepsilon) = \mathcal{E}_1(\varepsilon) + \mathcal{E}_2(\varepsilon)$ , with

$$\begin{aligned}\mathcal{E}_2(\varepsilon) &= \int_{B_\varepsilon(x^+)} f_0 (\Re\{v(x)\} - \Re\{v(x^+)\}) \, dx \\ &\quad - \int_{B_\varepsilon(x^-)} f_0 (\Re\{v(x)\} - \Re\{v(x^-)\}) \, dx = o(\varepsilon^2),\end{aligned}\quad (3.31)$$

where we have used the interior elliptic regularity of  $v$ . Thus, from the estimates (3.26) and (3.31), the expansion (3.30) allows us to set  $\rho(\varepsilon) = \pi\varepsilon^2$  in (3.1), leading to the main result of our work, namely:

**Theorem 4.** *The topological derivative of the shape functional (2.4) is given by*

$$D_T \psi(x) = f_0 \Re\{v(x)\} \times \begin{cases} +1, & \text{if } x \in \mathcal{W} \setminus \bar{\omega}, \\ -1, & \text{if } x \in \omega. \end{cases}\quad (3.32)$$

where  $v$  is solution to the adjoint Helmholtz equation (2.7).

**Remark 5.** *The obtained sensitivity (3.32) does not take into account for perturbations on the coefficients of the BVPs produced by the insertion/removal of antennas. However, such an incomplete sensitivity shall be useful for solving the topology optimization problem (2.5). In fact, we observe that the shape functional (2.4) is actually much more sensitive with respect to the source  $f(x)$  than to the other distributed parameters defined in  $\mathcal{W}$ . On the other hand, the derivation of the complete sensitivity with respect to all variable parameters is much more involved and somehow useless in this context.*

#### 4. A TOPOLOGY DESIGN ALGORITHM

In this section a topology optimization algorithm based on the obtained topological derivative (3.32) is devised. It consists basically in looking for a fixed-point for the minimization problem (2.5). For more sophisticated topology design algorithm, see for instance [34].

To present our topology optimization algorithm we introduce a domain representation function  $\Psi \in L^2(\Omega)$  such that

$$\Omega \setminus \omega = \{x \in \Omega : \Psi(x) = +1\}, \quad (4.1)$$

$$\omega = \{x \in \Omega : \Psi(x) = -1\}. \quad (4.2)$$

Therefore, the source  $f(x)$  can be defined through  $\Psi(x)$  as follows:

$$f(x) = \begin{cases} f_0, & \text{if } \Psi(x) = -1, \\ 0, & \text{if } \Psi(x) = +1, \end{cases} \quad (4.3)$$

Let us introduce  $\mathcal{W}^* \subset \mathcal{W}$  such that

$$\mathcal{W}^* = \{x \in \mathcal{W} : D_T\psi(x) < 0\}. \quad (4.4)$$

Additionally, the quantity

$$D_T\psi^* = \min_{x \in \mathcal{W}^*} D_T\psi(x) \quad (4.5)$$

is used to define  $\mathcal{W}^\beta \subset \mathcal{W}^*$  as follows

$$\mathcal{W}^\beta = \{x \in \mathcal{W}^* : D_T\psi(x) < (1 - \beta)D_T\psi^*\}, \quad (4.6)$$

where  $0 < \beta \leq 1$  induces a threshold for the topological derivative  $D_T\psi(x)$ . Finally, we introduce the function  $\Psi^\beta \in L^2(\Omega)$  associated with  $\beta$  as follows

$$\Psi^\beta(x) = \begin{cases} +\Psi(x), & \text{if } x \in \Omega \setminus \mathcal{W}^\beta, \\ -\Psi(x), & \text{if } x \in \mathcal{W}^\beta. \end{cases} \quad (4.7)$$

From these elements we can devise a simple topology optimization algorithm. The basic idea consists in insert/remove antenna by changing the sign of the domain representation function  $\Psi(x)$  according to the topological derivative  $D_T\psi(x)$ . In particular, we start with an initial guess  $\Psi_0$ . Then, for a generic iteration number  $n$ , we set  $\Psi_n = \Psi^\beta$  and update all quantities according to the new function  $\Psi_n$ . The procedure is repeated until a fixed point is found. The resulting topology design algorithm is summarized in the form of a pseudo-code presented in Algorithm 1, where  $\epsilon_{min}$  and  $\beta_{min}$  are given small tolerances.

---

**Algorithm 1:** The topology design algorithm
 

---

**input** : Initial guess  $\Psi_0$   
**output**: Optimal solution  $\Psi^*$

- 1  $n \leftarrow 0; \epsilon \leftarrow \epsilon_{min} + 1;$
- 2 **while**  $\epsilon > \epsilon_{min}$  **do**
- 3     Compute  $u_n, \theta_n, \psi_n;$
- 4     Compute  $\varphi_n, v_n;$
- 5     Compute  $D_T\psi_n, D_T\psi_n^*;$
- 6      $\beta \leftarrow 1, \psi_{old} \leftarrow \psi_n, \psi_n \leftarrow \psi_n + 1;$
- 7     **while**  $\psi_n > \psi_{old}$  **do**
- 8         Compute  $\mathcal{W}^\beta, \Psi^\beta;$
- 9          $\Psi_n \leftarrow \Psi^\beta;$
- 10        Execute line 3;
- 11        **if**  $\beta < \beta_{min}$  **then**
- 12             $\psi_n \leftarrow \psi_{old};$
- 13        **end if**
- 14         $\beta \leftarrow \beta/2;$
- 15     **end while**
- 16      $\epsilon \leftarrow \|\psi_n - \psi_{old}\|;$
- 17      $n \leftarrow n + 1;$
- 18 **end while**

---

## 5. NUMERICAL RESULTS

In this section some numerical experiments are presented, showing that the proposed optimization method can be potentially used in the treatment of cancer by hyperthermia. The first set of experiments presented in Section 5.1 is conducted to test the proposed optimization method, where the medium is assumed to be homogeneous. In Section 5.2, we apply the proposed optimization method to a model problem of a breast cancer treatment by hyperthermia, taking into account realistic heterogenous medium. The Galerkin finite element method is used to discretize the BVPs. To obtain stable Galerkin approximations to problems (2.2) and (2.7), a mesh of size  $h$  satisfying the condition  $k^2h < 1$  is adopted [35, 36]. In particular, the BVPs are discretized into a uniform mesh with  $400 \times 400$  square elements. Each square is then divided into eight triangles, so that the condition  $k^2h < 1$  holds true, where  $h$  is the finite element mesh size. In the pictures of the temperature distribution, the color levels black/brown to yellow/white mean colder to hotter.

**5.1. Experiment 1: Preliminary Tests .** In this first set of experiments, the computational domain is given by a square  $\Omega = (-1, 1) \times (-1, 1)$  as shown in Fig. 4. The healthy body  $\mathcal{B}$  is represented by a ball of radius  $\rho_{\mathcal{B}} = 0.2$ , while the diseased part of the body  $\mathcal{D}$  is given by a ball of radius  $\rho_{\mathcal{D}} = 0.04$ . The annular region with radii 0.3 and 0.6 represents the design domain for the antenna  $\omega$ . The weight  $\alpha$  of the shape functional is set as  $\alpha = 0.5$ . In all cases, the following parameters are adopted:  $\kappa = 1, c = 1, w = 1, \theta_b = 0, \theta_\Gamma = 0, f_0 = 1$  and  $r = 0$ . Finally, we set  $\sigma = 1$  in  $\mathcal{B}$  and  $\sigma = 0$  in the remainder part  $\mathcal{W} = \Omega \setminus \mathcal{B}$ . Note that all the properties are assumed to be homogeneous, except  $\sigma$ . In particular, there is no distinction between  $\mathcal{B}$  and  $\mathcal{D}$ . Therefore, the fictitious domain  $\mathcal{D}$  just represents the target region to be selectively heated.

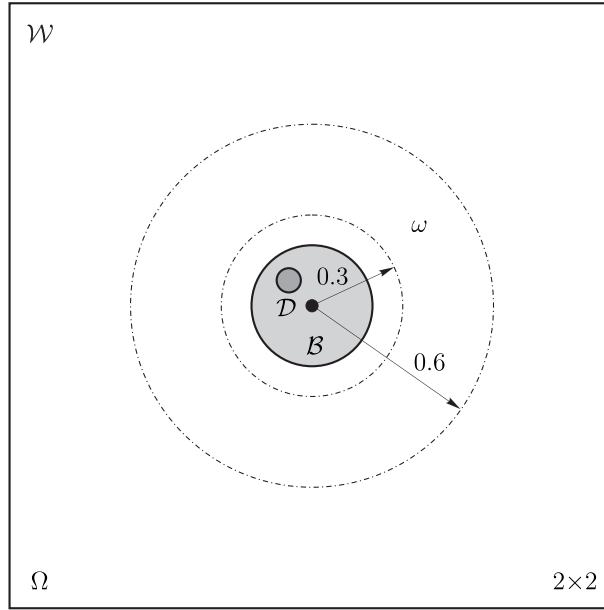


FIGURE 4. Sketch of Experiment 1.

5.1.1. *Example 1A.* In this example the target  $\mathcal{D}$  is positioned at the center of the body. The initial guess for the antenna  $\omega$  is given by a small ball of radius 0.04 and center at  $(-0.45, 0)$ . The experiments are driven by setting different wavenumbers  $k \in \{12, 16, 20\}$ . In all cases the target  $\mathcal{D}$  is heated independently of  $k$ , as can be seen through figs. 5, 6 and 7. However, the higher is the wavenumber the more focused becomes the temperature hot spot over the target  $\mathcal{D}$ .

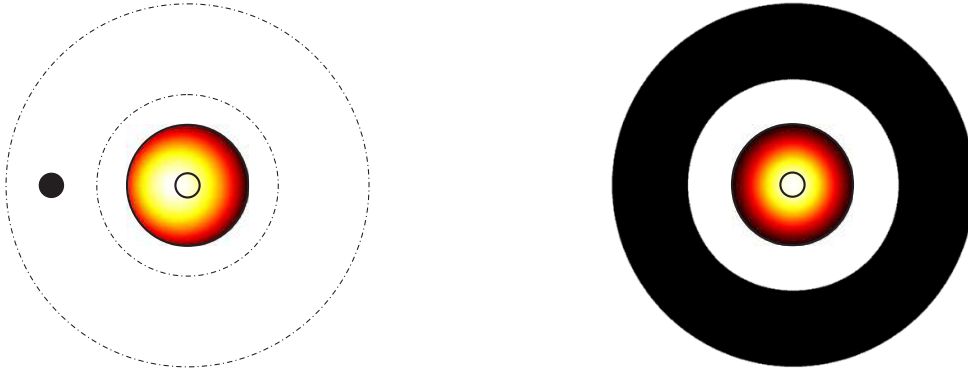


FIGURE 5. Example 1A: Experiment conducted with the wavenumber  $k = 12$ . On the left, is shown the initial configuration of the antenna  $\omega$  and initial temperature distribution in the body  $\mathcal{B}$ . On the right, is shown the final configuration of the antenna  $\omega$  and the final temperature distribution in the body  $\mathcal{B}$ , obtained after 8 iterations.

Let us now set the whole annular region with radii 0.3 and 0.6 as initial guess for the antenna  $\omega$ . We repeat the last experiment by setting the wavenumber  $k = 20$ . The obtained results are shown in Fig. 8. The optimal configuration obtained in the previous experiment (Fig. 7 left) is reproduced in Fig. 8 (left). In Fig. 8 we can also observe that the initial and final temperature distributions are qualitatively almost the same, because in this case the initial guess is also qualitatively close to the optimal solution (both are given by centered rings). We observed the same behavior for  $k$  equal to 12 and 16.

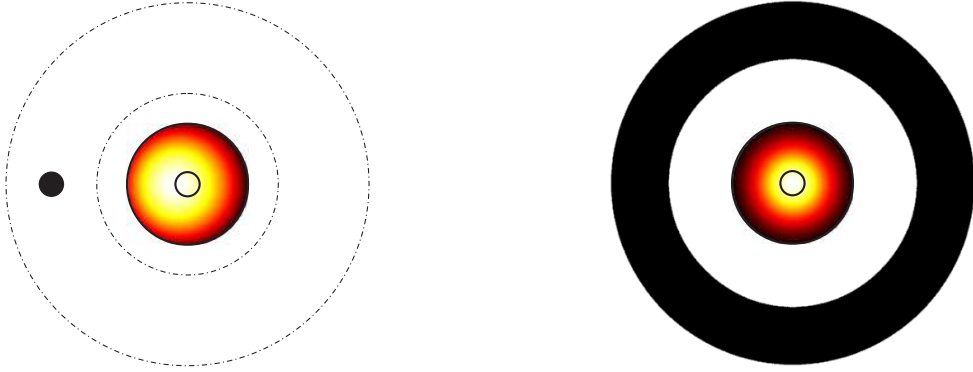


FIGURE 6. Example 1A: Experiment conducted with the wavenumber  $k = 16$ . On the left, is shown the initial configuration of the antenna  $\omega$  and initial temperature distribution in the body  $\mathcal{B}$ . On the right, is shown the final configuration of the antenna  $\omega$  and the final temperature distribution in the body  $\mathcal{B}$ , obtained after 18 iterations.

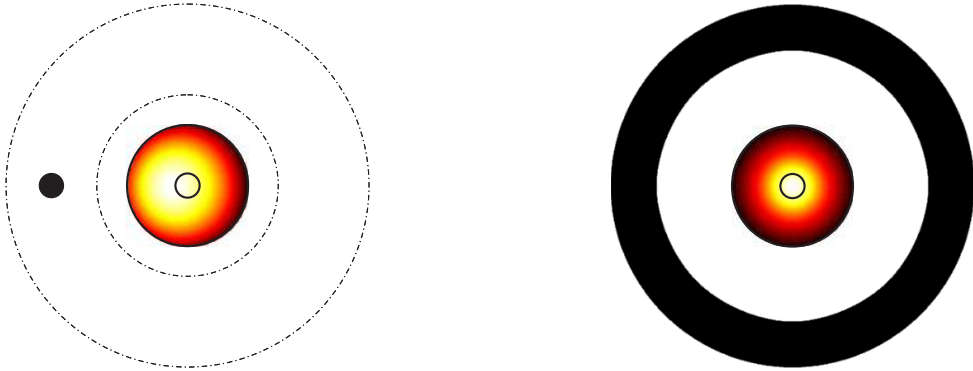


FIGURE 7. Example 1A: Experiment conducted with the wavenumber  $k = 20$ . On the left, is shown the initial configuration of the antenna  $\omega$  and initial temperature distribution in the body  $\mathcal{B}$ . On the right, is shown the final configuration of the antenna  $\omega$  and the final temperature distribution in the body  $\mathcal{B}$ , obtained after 33 iterations.

5.1.2. *Example 1B.* Now the target  $\mathcal{D}$  is positioned at  $(0.1, 0.1)$  and the initial guess for the antenna  $\omega$  is given by an annular region with radii 0.3 and 0.6, while the other parameters are the same as before. It is possible to observe that the results obtained with  $k$  equal to 12 and 16 are not satisfactory, as shown in Figs. 9 and 10, since the target has not been precisely heated. On the other hand, with  $k = 20$  the result is much better, as can be seen in Fig. 11.

We also set the initial guess for the antenna  $\omega$  as a small ball of radius 0.04 and center at  $(-0.45, 0)$  and repeat the last experiment by setting the wavenumber  $k = 20$ . The obtained results are shown in Fig. 12, showing a slightly different configuration for the antenna in comparison to the one presented on the right of Fig. 11. However, both temperature hot spots are concentrated over the target  $\mathcal{D}$ . The decay of the cost functionals at each iteration considering a small ball and a ring as initial guesses are shown in Fig. 13, where the value of the cost functional obtained for the ring (red) is 6% smaller than the one obtained from the ball (blue). See also Table 1.



FIGURE 8. Example 1A: Experiment conducted with the wavenumber  $k = 20$ . On the left, is shown the initial configuration of the antenna  $\omega$  and initial temperature distribution in the body  $\mathcal{B}$ . On the right, is shown the final configuration of the antenna  $\omega$  and the final temperature distribution in the body  $\mathcal{B}$ , obtained after 16 iterations.



FIGURE 9. Example 1B: Experiment conducted with the wavenumber  $k = 12$ . On the left, is shown the initial configuration of the antenna  $\omega$  and initial temperature distribution in the body  $\mathcal{B}$ . On the right, is shown the final configuration of the antenna  $\omega$  and the final temperature distribution in the body  $\mathcal{B}$ , obtained after 4 iterations.

TABLE 1. Example 1B: Experiments conducted with the wavenumber  $k = 20$ . Decay of the cost functional  $\psi_n$  ( $\times 10^{-8}$ ) at each iteration  $n$  considering a small ball and a ring as initial guesses.

	$\psi_0$	$\psi_1$	$\psi_2$	$\psi_3$	$\psi_4$	$\psi_5$
Ball	$7.75 \times 10^{-4}$	-11.58	-16.47	-16.99	-17.04	-17.05
Ring	$-208.14 \times 10^{-4}$	-7.96	-17.22	-18.09	-18.13	-18.14

**5.2. Experiment 2: A Breast Cancer Model .** In this numerical example, the problem is solved in a heterogeneous medium taking into account realistic data [13]. The computational domain is given by a square  $\Omega = (-0.5, 0.5) \times (-0.5, 0.5)$  [m<sup>2</sup>] as shown in Fig. 14. We suppose that the body  $\mathcal{B}$  represents a cross section of the human breast with radius  $\rho_{\mathcal{B}} = 0.075$  [m] and center at  $(0.0, 0.0)$ . The target to be heated  $\mathcal{D}$  represents a set of three tumors with radii and centers given respectively by  $\rho_{\mathcal{D}_1} = 0.005$  [m] and  $(-0.05, 0.03)$ ,  $\rho_{\mathcal{D}_2} = 0.010$  [m] and  $(0.03, 0.03)$ ,  $\rho_{\mathcal{D}_3} = 0.015$  [m] and  $(0.00, -0.04)$ . The domain  $\mathcal{W}$  is filled with deionized water. The annular region with radii 0.15 and 0.2

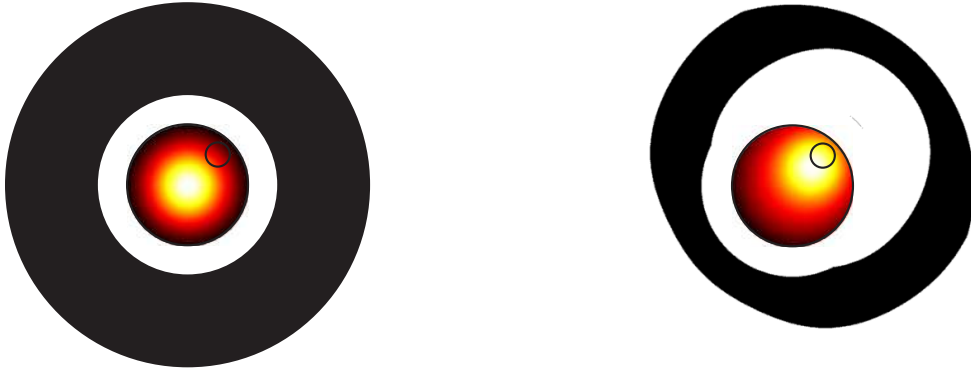


FIGURE 10. Example 1B: Experiment conducted with the wavenumber  $k = 16$ . On the left, is shown the initial configuration of the antenna  $\omega$  and initial temperature distribution in the body  $\mathcal{B}$ . On the right, is shown the final configuration of the antenna  $\omega$  and the final temperature distribution in the body  $\mathcal{B}$ , obtained after 8 iterations.



FIGURE 11. Example 1B: Experiment conducted with the wavenumber  $k = 20$ . On the left, is shown the initial configuration of the antenna  $\omega$  and initial temperature distribution in the body  $\mathcal{B}$ . On the right, is shown the final configuration of the antenna  $\omega$  and the final temperature distribution in the body  $\mathcal{B}$ , obtained after 5 iterations.

represents the design domain for the antenna  $\omega$ , whose initial guess is given by a small ball of radius 0.01 [m] and center at  $(-0.17, 0.00)$ . The weight  $\alpha$  of the shape functional is set as  $\alpha = 0.5$ .

The material properties for the semi-coupled system of variational equations (2.1)-(2.2) are described in Table 2 below. The relative permeability is set as  $\mu_r = 1$  in  $\Omega$ . The electrical and thermal properties of tissues and of the deionized water were found in [13]. The FR-4 antenna properties were found in [http://www.mtarr.co.uk/courses/topics/0140\\_p1/index.html](http://www.mtarr.co.uk/courses/topics/0140_p1/index.html), April, 2016.

In this experiment all coefficients of the body (electrical as well as thermal) have been corrupted with 10% of white Gaussian noise. To show the difference between the original and noisy properties, we plot in Fig. 15 the thermal conductivity  $\kappa$  of the breast  $\mathcal{B}$  without noise (left) and with noise (right).

To solve this problem we apply a frequency of 140 [MHz] [13]. The temperature of the background is set as  $\theta_b = 36^\circ C$ , while the boundary conditions for the thermal and electromagnetic problems are given by  $\theta_\Gamma = 36^\circ C$  and  $r = 0$ , respectively. The computational domain  $\Omega$  is discretized into a uniform grid with  $600 \times 600$  square elements

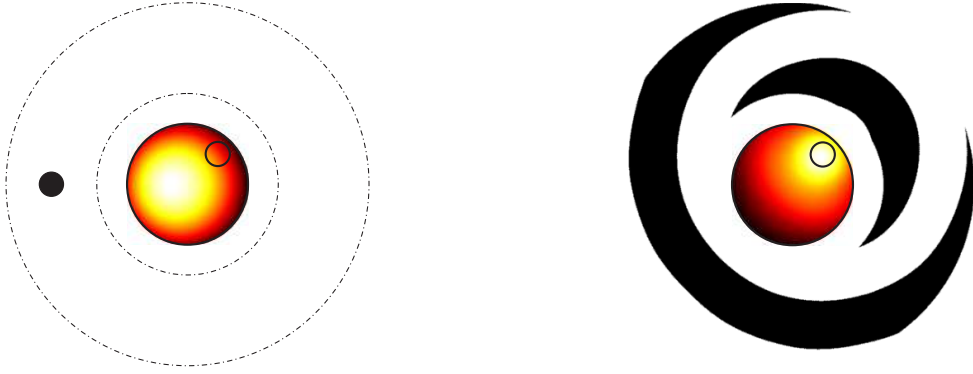


FIGURE 12. Example 1B: Experiment conducted with the wavenumber  $k = 20$ . On the left, is shown the initial configuration of the antenna  $\omega$  and initial temperature distribution in the body  $\mathcal{B}$ . On the right, is shown the final configuration of the antenna  $\omega$  and the final temperature distribution in the body  $\mathcal{B}$ , obtained after 5 iterations.

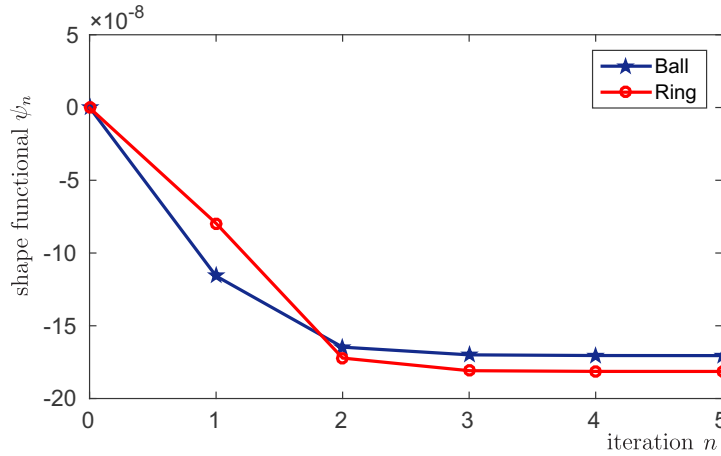


FIGURE 13. Example 1B: Experiments conducted with the wavenumber  $k = 20$ . Decay of the cost functional  $\psi_n$  at each iteration  $n$  considering a small ball (blue) and a ring (red) as initial guesses.

TABLE 2. Material Properties of Experiment 2.

Properties	Region	$\varepsilon_r$	$\sigma$	$\kappa$	$c$	$w$
Fat	$\mathcal{B} \setminus \overline{\mathcal{D}}$	20.4	0.12	0.22	2387	1.1
Tumor	$\mathcal{D}$	65	0.78	0.56	3639	1.8
Water	$\mathcal{W}$	76.5	$10^{-3}$	0.50	4178	0.0
Antenna	$\omega$	4.5	0.0	0.27	0.0	0.0

with each resulting square divided into eight triangles, so that the condition  $k^2h < 1$  is fulfilled.

The idea is to heat one tumor by once. The electromagnetic intensity  $f_0$  used to heat each tumor individually is given in Table 3. The initial temperature distributions are always quasi-uniform about  $36^\circ C$ . In Fig. 16 we show the final configuration of the antenna  $\omega$  (in black) and the final temperature distribution in the breast  $\mathcal{B}$  (in color) for each target. The number of iterations for each case is also shown in Table 3.

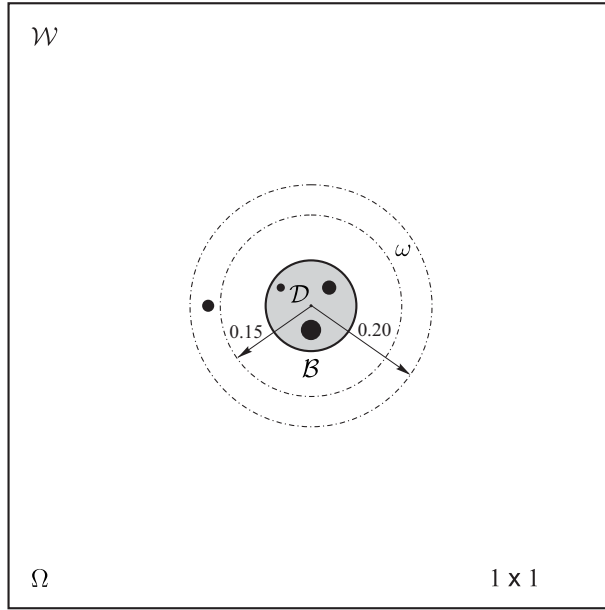


FIGURE 14. Sketch of Experiment 2.

FIGURE 15. Experiment 2: Thermal conductivity  $\kappa$  of the breast  $\mathcal{B}$  without noise (left) and with 10% of white Gaussian noise (right).

TABLE 3. Additional data of Experiment 2.

	radius	center	$f_0 (\times 10^6)$	iterations
Case #1	0.005	(-0.05, 0.03)	400	4
Case #2	0.010	( 0.03, 0.03)	220	12
Case #3	0.015	( 0.00, -0.04)	180	14

Note that the perturbations on the coefficients of the BVPs produced by the insertion/removal of antennas are not taken into account by the sensitivity formula (3.32). On the other hand, these properties were updated during the iterative process. Therefore, this procedure can be seen as a *sensitivity delay* in the pseudo-time  $n$  in Algorithm 1. As expected in Remark 5, such an incomplete sensitivity has been able to properly minimize the shape function. In fact, from an inspection of Fig. 16, we observe in all cases that the cancer  $\mathcal{D}$  is heated over  $42^\circ\text{C}$ , while keeping the temperature in the healthy body under  $39^\circ\text{C}$ .

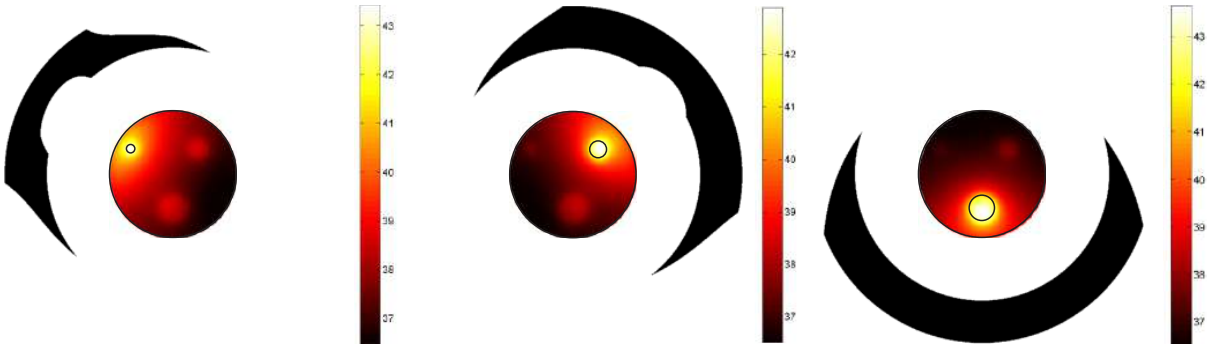


FIGURE 16. Experiment 2: Final configuration of the antenna  $\omega$  and final temperature distribution in the breast  $\mathcal{B}$  (center). On the left, center and right we present the results for the smallest ( $\rho_{\mathcal{D}_1} = 0.005$ ), medium ( $\rho_{\mathcal{D}_2} = 0.010$ ) and biggest ( $\rho_{\mathcal{D}_3} = 0.015$ ) tumors, respectively. The hot spots are always concentrated in the corresponding tumor, leading to a temperature over  $42^\circ\text{C}$  in all cases.

## 6. CONCLUSIONS

A new method for topology optimization design of antenna applied to the treatment of cancer by hyperthermia is proposed based on the topological derivative concept. As the hyperthermia problem is modeled by a semi-coupled system of partial differential equations, two nested adjoint problems have been introduced in order to simplify the form of the topological derivative, leading to a point-wise formula easy to implement. Based on the obtained theoretical result a fixed-point algorithm has been devised, which converges to a solution of the problem in very few iterations. The results presented here on some preliminary numerical simulations indicate that the proposed methodology is very promising to the design of electromagnetic antennas to selectively heat a target region. In particular, we have presented an experiment concerning breast cancer hyperthermia where the cancer has been heated over  $42^\circ\text{C}$ , while the temperature in the healthy body has been kept under  $39^\circ\text{C}$ . These results are in agreement with the initial motivation for our work.

**Acknowledgments.** This research was partly supported by CNPq (Brazilian Research Council), CAPES (Brazilian Higher Education Staff Training Agency) and FAPERJ (Research Foundation of the State of Rio de Janeiro). These supports are gratefully acknowledged.

## REFERENCES

- [1] M. E. Kowalski, B. Behnia, A. G. Webb, J. Jian-Ming, Optimization of electromagnetic phased-arrays for hyperthermia via magnetic resonance temperature estimation, *IEEE Transactions on Biomedical Engineering* 49 (11) (2002) 1229–1241.
- [2] A. Chichel, J. Skowronek, M. Kubaszewska, M. Kanikowski, Hyperthermia - description of a method and a review of clinical applications, *Reports of Practical Oncology and Radiotherapy* 12 (5) (2007) 267–275.
- [3] G. Hegyi, G. Szigeti, A. Szász, Hyperthermia versus oncothermia: Cellular effects in complementary cancer therapy, *Evidence-Based Complementary and Alternative Medicine* 2013 (2013) 1–12.
- [4] R. B. Roemer, Engineering aspects of hyperthermia therapy, *Annual Review of Biomedical Engineering* 1 (1999) 347–376.
- [5] R. B. Roemer, T. C. Cetas, J. R. Oleson, S. Halac, A. Y. Matloubieh, Comparative evaluation of hyperthermia heating modalities: I. numerical analysis of thermal dosimetry bracketing cases, *Radiation Research* 100 (3) (1984) 450–472.

- [6] J. Lang, B. Erdmann, M. Seebass, Impact of nonlinear heat transfer on temperature control in regional hyperthermia, in: *IEEE Trans. on Biomedical Engineering*, 1997, pp. 97–73.
- [7] K. D. Paulsen, S. Geimer, J. Tang, W. E. Boyse, Optimization of pelvic heating rate distributions with electromagnetic phased arrays, *International Journal of Hyperthermia* 15 (3) (1999) 157–186.
- [8] H. Kroeze, J. B. V. de Kamer, A. A. C. D. Leeuw, J. J. W. Lagendijk, Regional hyperthermia applicator design using FDTD modelling, *Physics in Medicine and Biology* 46 (7) (2001) 1919–1935.
- [9] M. Henke, W. T. Joines, T. V. Samulski, Variations of focal regions versus numbers and positions of sources in two-dimensional media, *International Journal of Hyperthermia* 17 (5) (2001) 382–400.
- [10] M. Seebass, R. Beck, J. Gellermann, J. Nadobny, P. Wust, Electromagnetic phased arrays for regional hyperthermia: optimal frequency and antenna arrangement, *International Journal of Hyperthermia* 17 (4) (2001) 321–336.
- [11] H. P. Kok, P. M. A. V. Haaren, J. B. V. de Kamer, J. Wiersma, J. D. P. V. Dijk, J. Crezee, High-resolution temperature-based optimization for hyperthermia treatment planning, *Physics in Medicine and Biology* 50 (13) (2005) 3127–3141.
- [12] M. Converse, E. J. Bond, B. D. Veen, S. C. Hagness, A computational study of ultra-wideband versus narrowband microwave hyperthermia for breast cancer treatment, *IEEE Transactions on Microwave Theory and Techniques* 54 (5) (2006) 2169–2180.
- [13] L. Wu, R. J. McGough, O. A. Arabe, T. V. Samulski, An RF phased array applicator designed for hyperthermia breast cancer treatments, *Physics in Medicine and Biology* 51 (1) (2006) 1–20.
- [14] J. Oden, K. Diller, C. Bajaj, J. Browne, J. Hazle, I. Babuška, J. Bass, L. Biduat, L. Demkowicz, A. Elliott, Y. Feng, D. Fuentes, S. Prudhomme, M. N. Rylander, R. Stafford, Y. Zhang, Dynamic data-driven finite element models for laser treatment of cancer, *Numerical Methods for Partial Differential Equations* 23 (4) (2007) 904–922.
- [15] Y. Feng, D. Fuentes, A. Hawkins, J. Bass, M. Rylander, A. Elliott, A. Shetty, R. Stafford, J. Oden, Nanoshell-mediated laser surgery simulation for prostate cancer treatment, *Engineering with Computers* 25 (1) (2009) 3–13.
- [16] P. F. Maccarini, K. Arunachalam, C. D. Martins, P. R. Stauffer, Size reduction and radiation pattern shaping of multi-fed DCC slot antennas used in conformal microwave array hyperthermia applicators, Vol. 7181, 2009, pp. 1–16.
- [17] H. D. Trefná, J. Vrba, M. Persson, Time-reversal focusing in microwave hyperthermia for deep-seated tumors, *Physics in Medicine and Biology* 55 (8) (2010) 2167–2185.
- [18] D. T. Tompkins, R. Vanderby, S. A. Klein, W. A. Beckman, R. A. Steeves, D. M. Frye, B. R. Paliwal, Temperature-dependent versus constant-rate blood perfusion modelling in ferromagnetic thermoseed hyperthermia: results with a model of the human prostate, *International Journal of Hyperthermia* 10 (4) (1994) 517–536.
- [19] R. A. da Silva, Modelagem computacional de espalhamento de ondas eletromagnéticas, Ph.D. thesis, Laboratório Nacional de Computação Científica (2011).
- [20] M. P. Bendsøe, O. Sigmund, *Topology optimization. Theory, methods and applications*, Springer-Verlag, Berlin, 2003.
- [21] J. A. Sethian, *Level Set Methods and Fast Marching Methods: Evolving Interfaces in Computational Geometry, Fluid Mechanics, Computer Vision, and Materials Science*, Cambridge University Press, Cambridge, UK, 1999.
- [22] A. A. Novotny, J. Sokołowski, *Topological derivatives in shape optimization, Interaction of Mechanics and Mathematics*, Springer, 2013.
- [23] J. Sokołowski, A. Żochowski, On the topological derivative in shape optimization, *SIAM Journal on Control and Optimization* 37 (4) (1999) 1251–1272.
- [24] S. Amstutz, A. A. Novotny, Topological optimization of structures subject to von Mises stress constraints, *Structural and Multidisciplinary Optimization* 41 (3) (2010) 407–420.
- [25] A. Carpio, M.-L. Rapún, Solving inhomogeneous inverse problems by topological derivative methods, *Inverse Problems* 24 (4) (2008) 045014.
- [26] M. Hintermüller, A. Laurain, Multiphase image segmentation and modulation recovery based on shape and topological sensitivity, *Journal of Mathematical Imaging and Vision* 35 (2009) 1–22.
- [27] S. Amstutz, S. M. Giusti, A. A. Novotny, E. A. de Souza Neto, Topological derivative for multi-scale linear elasticity models applied to the synthesis of microstructures, *International Journal for Numerical Methods in Engineering* 84 (2010) 733–756.
- [28] N. Van Goethem, A. A. Novotny, Crack nucleation sensitivity analysis, *Mathematical Methods in the Applied Sciences* 33 (16) (2010) 197–1994.

- [29] G. Allaire, F. Jouve, N. Van Goethem, Damage and fracture evolution in brittle materials by shape optimization methods, *Journal of Computational Physics* 230 (12) (2011) 5010–5044.
- [30] J. Melenk, On Generalized Finite Element Methods, PhD Thesis, University of Maryland at College Park, 1995.
- [31] S. Sauter, A refined finite element convergence theory for highly indefinite Helmholtz problems, *Computing* 78 (2) (2006) 101–115.
- [32] L. Banjai, S. Sauter, A refined Galerkin error and stability analysis for highly indefinite variational problems, *SIAM Journal on Numerical Analysis* 45 (1) (2007) 37–53.
- [33] R. Dautray, J. L. Lions, *Mathematical analysis and numerical methods for science and technology. Volume 2 – Functional and Variational Methods*, Springer, Berlin, Heidelberg, New York, 1988.
- [34] S. Amstutz, H. Andrä, A new algorithm for topology optimization using a level-set method, *Journal of Computational Physics* 216 (2) (2006) 573–588.
- [35] F. Ihlenburg, I. M. Babuska, Finite element solution of the Helmholtz equation with high wave number Part I: The h-version of the fem, *Computers & Mathematics with Applications* (30, issue 9) (1995) 9–37.
- [36] F. Ihlenburg, I. Babuska, Dispersion analysis and error estimation of Galerkin finite element methods for the Helmholtz equation, *International Journal for Numerical Methods in Engineering* 38 (22) (1995) 3745–3774.

(Amad et al.) LABORATÓRIO NACIONAL DE COMPUTAÇÃO CIENTÍFICA LNCC/MCT, COORDENAÇÃO DE MATEMÁTICA APLICADA E COMPUTACIONAL, AV. GETÚLIO VARGAS 333, 25651-075 PETRÓPOLIS - RJ, BRASIL

*E-mail address:* novotny@lncc.br